Performance Analysis of Electrostatic Switched Radiator Using Heat-Flux-Based Emissivity Measurement

Joseph Currano,* Saeed Moghaddam,† and John Lawler‡
Advanced Thermal and Environmental Concepts, College Park, Maryland 20740
and
Kim Jungho§
University of Maryland, College Park, Maryland 20742

DOI: 10.2514/1.35960

The heat-flux-based emissivity measurement technique developed in our earlier work has been used to study the performance of an electrostatic switched radiator. The capability of fast and accurate measurement of the real-time changes in emissivity enabled by this technique allowed understanding of the transient behavior during activation, as well as identification of a major failure mode of the second-generation electrostatic radiator. A solution for resolution of this failure mode was then proposed and successfully tested, producing accurate and repeatable results over many cycles. A change in emissivity of 0.52 was achieved with 280 V applied, among the best consistent results achieved through electrostatic technology. The current work offers further understanding of electrostatic radiator performance and its application to space vehicles.

Nomenclature

A	=	area
F	=	view factor
q	=	heat transfer rate, W
q''	=	heat flux, W/m^2
T	=	temperature, K
ε	=	emissivity
σ	=	Stefan–Boltzmann constant

Subscripts

S	=	surface
1, 2	=	generic surfaces
1–2	=	from surface 1 to surface 2
∞	=	far field

Introduction

FUTURE satellites are expected to be significantly smaller, lighter, more energy efficient, and more cost effective than existing satellites. Among the technologies being developed to enable such benefits are radiators with variable emissivity coatings. Recent studies [1,2] have suggested that variable emissivity radiators offer substantial weight and energy savings over current thermal control systems (e.g., variable conductance heat pipe, large heaters, and mechanical louvers). The new variable emissivity systems allow rapid variation of the radiator emissivity to control heat dissipation from the satellite. Several concepts have been proposed in recent years. In general, these concepts can be broadly classified into two categories: changing the optical properties of the emitting surface and modifying the surface structurally to alter its radiation heat transfer performance. Polymer-based materials [3] and inorganic thin films [4,5] are two examples of surfaces with variable optical properties, which are used in electrochromic emissivity control. Two structurally active surfaces under development are microelectromechanical sensor (MEMS) louvers [6] and electrostatic switched radiator (ESR) [7,8]. MEMS louvers are microfabricated versions of the larger scale louvers that were developed earlier for spacecraft, allowing radiation when open and shielding the radiation when closed. An ESR operates in vacuum by opening and closing a gap between two surface layers via electrostatic forces, with the gap hindering heat transfer through the surface layers. The effective emissivity is controlled by coating the base layer with a low emissivity surface and the top layer with a high emissivity surface. When a voltage is applied, the top layer is electrostatically attracted to the base layer allowing heat to conduct into the top layer, so that the effective emissivity is approximately that of the top layer. In the deactivated state, the gap between the layers minimizes conduction. Heat must radiate from the base layer to the top layer before radiating outward, and so the effective emissivity is closer to that of the base layer.

The structurally active surfaces (i.e., MEMS louvers and ESRs) are further along in the development process than electrochromic emissivity control techniques. The first-generation devices tested recently onboard NASA's Space Technology 5 (ST-5) satellite, however, suggested an emissivity variation of only about 0.03 for MEMS louvers [9]. Further development efforts are evidently necessary to improve the performance of MEMS louvers before they can be implemented in future space vehicles. The ESR showed much better performance with an emissivity variation range of about 0.33 with an applied voltage of 350 V. This difference in emissivity was inferred from changes in amplitude of the temperature variation cycles of the ESR structure between the off and on states. Unfortunately, an important deficiency in this experiment was the method used for evaluation of the ESR performance. Variations in the satellite's orbit, thermal transients within the test structure, and incomplete deactivation of the ESR during the off cycle (as described later) may have all introduced significant errors in the estimation of the emissivity change upon activation. Furthermore, the tests did not provide any understanding about the transient behavior of the ESR device, which requires an emissivity measurement technique with a fast response time.

Recent development of the heat-flux-based (HFB) emissivity measurement technique [10,11] has provided an opportunity to accurately characterize and enhance the ESR technology. As

Received 30 November 2007; revision received 12 February 2008; accepted for publication 12 February 2008.

*Laboratory Engineer, 7100 Baltimore Avenue, Suite 300.
†Vice President of Research and Development, 7100 Baltimore Avenue, Suite 300.
‡President, 7100 Baltimore Avenue, Suite 300.
§Associate Professor, Department of Mechanical Engineering, 2181 Martin Hall.

mentioned in [12], a second generation ESR device is expected to be flown as part of the sixth Materials International Space Station Experiment (MISSE-6) which is scheduled to be installed by a space shuttle crew on the exterior of the International Space Station in 2008. ATEC, Inc. and Sensortex, Inc. have been working together over the past two years on preparation of the MISSE-6 flight module and on advancing the ESR technology. This paper describes using the HFB emissivity technique to characterize the performance improvement (i.e., lower operation voltage, greater change in emissivity, and more reliable operation) of the second generation ESR device.

Heat Flux-Based Emissivity Measurement

Details of the HFB measurement technique and its advantages over traditional emissivity measurement techniques have been described in an earlier study [11]. In this technique, a heat flux sensor installed beneath the emitting surface provides a direct measurement of the heat flow through the emitting surface. The heat flux passing through the surface, the surface temperature, and the ambient temperature are then used to calculate emissivity from the Stefan–Boltzmann law:

$$\varepsilon = \frac{q''}{\sigma\left(T_S^4 - T_\infty^4\right)} \tag{1}$$

Two aspects of this technique that are very well suited for testing variable emissivity surfaces are the fast response time and the ability to measure emissivity in a configuration in which the active surface is part of the vehicle structure (i.e., the HFB technique is insensitive to parasitic losses).

Integration of Heat Flux Sensor into Electrostatic Switched Radiator Structure

A test module incorporating a 50.8×50.8 mm heat flux sensor, custom made by RdF Corporation, and an ESR device was assembled by Sensortex, Inc. A schematic diagram showing a cross section of the test module is shown in Fig. 1. It is built on a $52.8 \times 52.8 \times 4.78$ mm aluminum substrate. The heat flux sensor was attached to the substrate using a film epoxy, and a thin (0.813 mm) aluminum plate was epoxied to the top of the heat flux sensor. The aluminum plate had a tab at one corner, so that a voltage lead could be attached to activate the ESR. An electrically insulating film consisting of a mixture of $BaTiO_3$ and Imron 3.4 HG-C polyurethane paint, was spray deposited onto the aluminum plate to a thickness of approximately 25 μm. The ESR membrane was attached to the insulating layer at the corners using 0.1-mm-thick pressure sensitive adhesive such that the elasticity of the membrane caused it to be suspended loosely over the insulator when the ESR was not actuated. With a ground lead attached to the metallized, low-ε backside of the membrane and a high voltage applied to the lead attached to the aluminum plate, the ESR was actuated and the membrane clung tightly to the surface, changing the heat transfer mode between the membrane and the surface beneath it from radiation to conduction. In this mode, the effective emissivity of the device was close to the emissivity of the front side of the membrane.

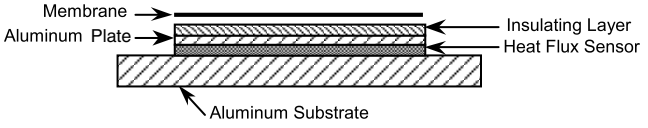

Fig. 1 Schematic of the ESR and heat flux sensor assembly.

The differences between the first- and second-generation ESRs are in the insulator and the membrane. In the first-generation ESR, the insulator function was built into the membrane, which was a polyimide film (insulator) metallized on the top surface (electrode), then painted with a high-emissivity paint [12]. In the second-generation ESR, the insulator function was shifted to the base and the metallized layer was on the bottom surface of the membrane, so that the electric field was no longer across the membrane. The polyurethane paint insulator has a greater dielectric constant than the polyimide layer used in the first-generation device, providing greater electrostatic attraction between the base and the membrane during the activation mode. The membrane was also made thinner in the second-generation ESR to enhance its flexibility and was impregnated with carbon particles to raise its surface charge conduction as well as its emissivity.

Two ESR devices with integrated heat flux sensors were fabricated and installed on a flight package designed for the MISSE-6 space experiment. Figure 2 shows a front view of the MISSE-6 package. In addition to the two ESR devices, four small heat flux sensors were installed on the package with paints and other passive coatings. The passive coatings have known emissivities and serve as reference surfaces. The package consists of an aluminum enclosure that holds the flight electronics (for voltage supply and data acquisition) and is also equipped with two photodiodes to measure approximately the intensity of the incoming radiation. Two thermocouples are attached to the inside of the enclosure to measure the surface temperature. During the ground test, the flight electronics were not used and the outputs of the heat flux sensors and thermocouples were recorded using a laboratory data acquisition system.

Experimental Setup

Two additional thermocouples were installed on the outside of the aluminum enclosure of the MISSE-6 package to measure its temperature during the ground test. Three film heaters were attached to the sides of the enclosure to control its temperature during the test. The MISSE-6 package was installed inside a vacuum chamber as described in [11]. The lid had four sets of feedthroughs allowing for connection of thermocouples, heat flux sensors, power for the heaters, and the excitation voltage of the two ESRs. The chamber was evacuated to a pressure of 10^{-8} bar or lower to reduce the effective thermal conductivity of air to 0.8% of its value at atmospheric pressure [13,14], thus eliminating conduction from the heated surface to the remaining gas. A Teflon rod suspended from the chamber lid was used to hold a $1/8$ in. (0.32 cm) thick copper plate to

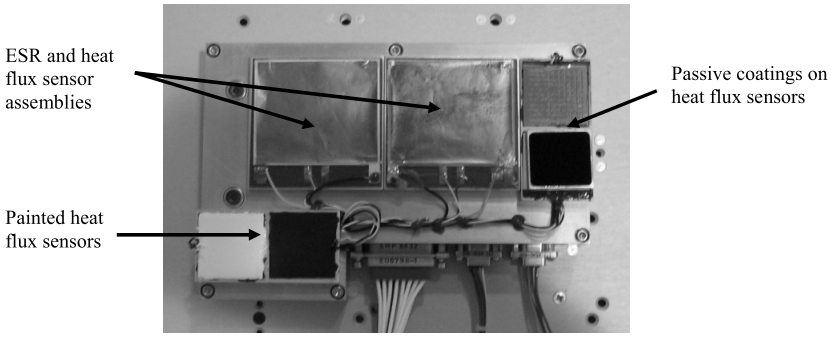

Fig. 2 Two ESR and heat flux sensor assemblies on MISSE-6 flight module.

Fig. 3 Vacuum chamber lid, feedthroughs, and MISSE-6 assembly.

which the MISSE-6 flight module was bolted. Figure 3 shows the assembly consisting of the chamber lid, feedthroughs, and the MISSE-6 assembly. Once the vacuum chamber was fully assembled, it was suspended inside a liquid nitrogen Dewar flask to fix the wall temperature at −195°C. A data acquisition system with a software interface was used to record the temperature and heat flux sensor readings.

The inside of the vacuum chamber was coated with a black paint whose emissivity is about 0.90, as measured optically by Sheldahl Corporation (now Multek Flexible Circuits, Inc.). A cone was fabricated and attached to the bottom of the chamber to increase the likelihood of multiple reflections before the emitted radiation returned to the substrate. However, assuming the cone and wall to be diffuse emitters, it was still possible that some reflection would reach the test surface. This was accounted for by the fact that the area of the sample surface was much smaller than the inside surface of the chamber, so that the test surface was effectively radiating to a blackbody at liquid nitrogen temperature (−195°C) when the Dewar was full. The heat flux from the test surface to the enclosure can be written as a two-node, source-sink radiation network [15]:

$$q_{1\text{–}2} = \frac{\sigma T_1^4 - \sigma T_2^4}{(1-\varepsilon_1/\varepsilon_1 A_1) + (1/A_1 F_{1\text{–}2}) + (1-\varepsilon_2/\varepsilon_2 A_2)} \tag{2}$$

where surface 1 is the test surface and surface 2 is the inner wall of the vacuum chamber (including the cone). Since $F_{1\text{–}2} = 1$, and if $A_2 \gg A_1$, the equation reduces to

$$q_{1\text{–}2} = \left(\sigma T_1^4 - \sigma T_2^4\right)\varepsilon_1 A_1 \tag{3}$$

which describes the heat flux from a surface emitting to a blackbody, and is the same as Eq. (1). For the ESR radiating to the chamber wall, $A_2 \approx 90A_1$, and so this arrangement adequately simulates radiation to a blackbody. An approximation of the numerical error due to this blackbody assumption is given in the Uncertainty Analysis section to follow.

Experimental Procedure

The Dewar flask was gradually charged with liquid nitrogen. Less than 1 h was required for the entire vacuum chamber assembly to reach liquid nitrogen temperature (−195°C), as indicated by five thermocouples installed at different locations on the internal surface of the vacuum chamber basin and lid. The electrical power applied to the heaters was controlled using a PID system to set the temperature of the test module at the desired level. The module temperature and the output of the heat flux sensors were then recorded as the ESR devices were switched on and off. The chamber pressure in all tests was less than 10^{-8} bar (7.5×10^{-6} torr).

Test Results and Discussions

Preliminary tests revealed a major ESR operational failure mode. The apparent emissivity often did not drop to the expected low value (i.e., 0.2–0.3) immediately after the applied voltage was turned off. Visual observation of the ESR device outside the test chamber revealed that the ESR membrane would remain in contact with the substrate after the voltage was removed. This "sticking" behavior caused the heat flux readings to drop much more slowly, sometimes taking hours to reach the preactivation value. Further investigations showed that this behavior occurred after the ESR device had been cycled many times or after it was left activated for a period longer than several minutes. Figure 4 illustrates an example of this problem. In this case, 300 V was applied to the ESR in three 1 h on/1 h off cycles, and was left off after the third cycle. The high emissivity value here was 0.94 and the fully deactivated value was 0.27 ($\Delta\varepsilon = 0.67$). This 0.67 variation is consistent with the result presented in [11] for an ESR with a Kapton insulator actuated at 315 V. However, as shown by the slow decline in emissivity, the membrane did not fully release until hours after the device was turned off.

It was hypothesized that the sticking was caused by the very long time required to return to electrical neutrality (i.e., relaxation) after charge injection/extraction or reorientation of the dipoles in the insulating layer caused by the applied electric field. To neutralize the charge and force relaxation, it was proposed to apply briefly a reversed polarity to the ESR device. The efficacy of this procedure is demonstrated with another pair of ESRs (same model) in Fig. 5. After

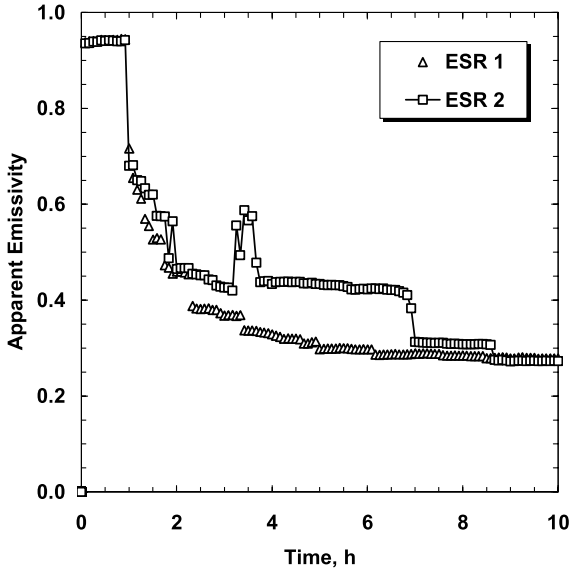

Fig. 4 Effective emissivity of two ESR devices as a function of time. The membranes did not fully release until hours after deactivation.

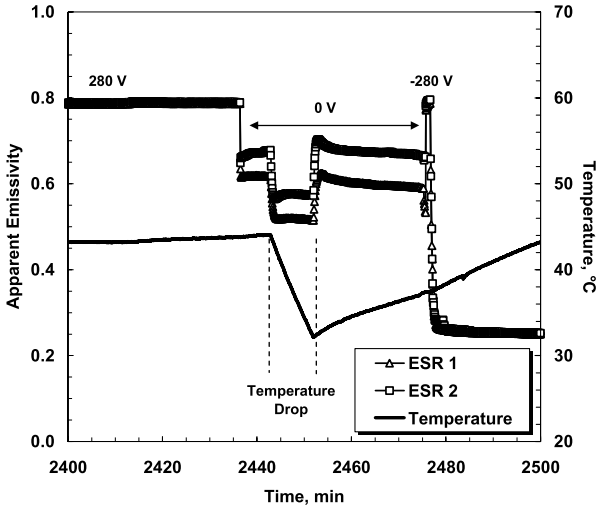

Fig. 5 Effective emissivity of two ESRs as a function of time. The membrane released after the polarity was reversed for 1 min. (The temporary drop is caused by the sudden temperature change.)

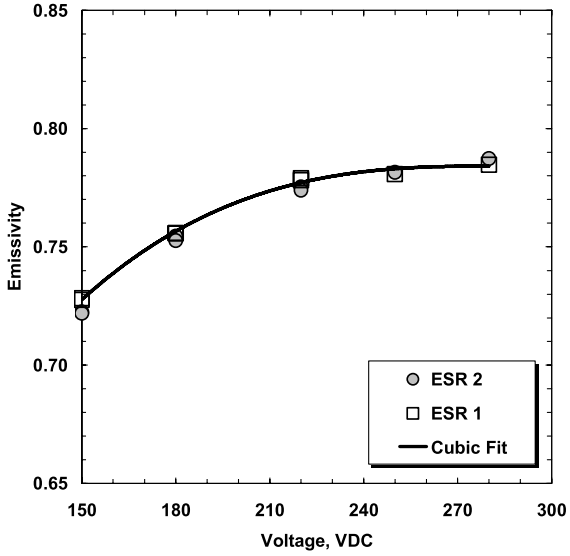

Fig. 6 Emissivity in activated state of second-generation ESR vs applied voltage.

removing the 280 V activation voltage (at about the 2435 min mark) both ESR devices only deactivated partially, with their apparent emissivities dropping from 0.8 to 0.6–0.7. This sticking or partial deactivation continued for about 40 min, at which time the reverse polarity voltage was applied for 1 min. Initially, the emissivity increased back to the activated value of 0.8, because the ESR devices can be activated by voltages of either polarity. However, when the reversed polarity voltage was removed, the apparent emissivities of both ESR devices dropped very quickly to an emissivity of about 0.25 (total variation of 0.55).

After fixing the problem of sticking, two additional tests were conducted to further characterize the ESR performance. First, the applied voltage was varied in five steps from 150 to 280 V, and the emissivity was measured for each voltage as shown in Fig. 6. A significant change in the emissivity of the activated state was determined in an applied voltage range of 150–220 V, but the slope in the emissivity vs voltage curve was much smaller beyond 220 V. The nonactivated emissivity for these ESRs was about 0.25–0.30, with activated emissivity values of 0.72 at 150 V to 0.78 at 280 V, giving a change in emissivity between off and on states in the range of 0.43–0.52 for these voltages. Later runs at the same voltages were consistent with these results.

A second test was conducted to study transient behavior of the ESR upon activation. Test results showed that when the ESR was activated, the heat flux sensor reading showed a spike in the heat flux (see Fig. 7) which then dropped to a lower steady-state value over several seconds. When the heat flux data were converted to emissivity, this spike appeared as a jump in the apparent emissivity to a value greater than one, followed by a gradual drop to a steady-state value close to the emissivity of the membrane material. The activated emissivity in this test was 0.8, and the low emissivity was 0.37, for a total variation of 0.43. The low emissivity value was higher than usual because very little time was allowed between activation cycles ($\sim$1 min).

This behavior is believed to result from a combination of the increased radiation from the ESR and a transient portion due to sensible heating of the membrane by conduction from the rest of the ESR. The main body of the ESR was continually in good thermal contact with the substrate, whereas the membrane in its relaxed state was somewhat thermally isolated from the substrate and thus at a lower temperature than the rest of the ESR. When the ESR was activated, a sudden spike in heat flux occurred because of the sensible heating of the membrane required to bring it to the temperature of the

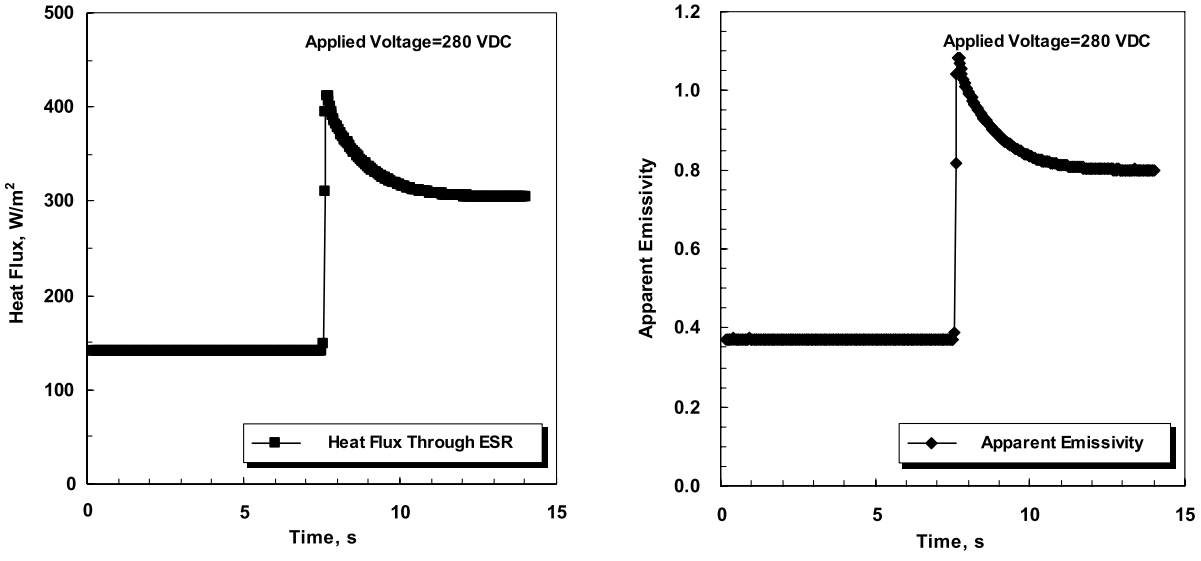

a) b)

Fig. 7 Transient behavior of the ESR upon activation at 280 V with a module temperature of 13°C.

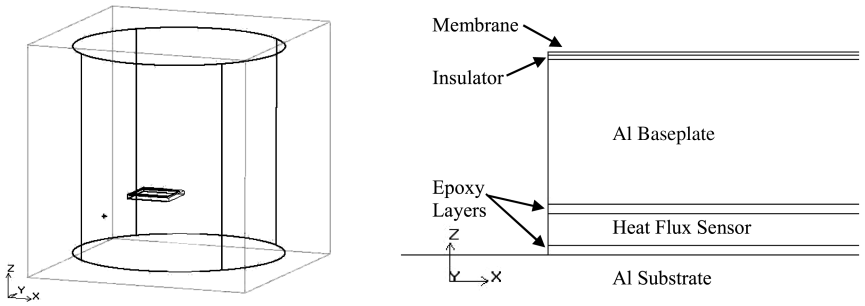

Fig. 8 Numerical model of ESR showing a) entire model and b) close up of ESR layers.

substrate. The steady-state heat flux was established after activation due to the high emissivity of the membrane which was then in good thermal contact with the substrate, causing a high effective emissivity.

To further analyze this transient behavior, a numerical model of the ESR and test chamber was built using Icepak software to predict the heat flux upon activation of the ESR. The ESR was modeled with the membrane in contact with the insulator/baseplate, with an initial membrane temperature lower than that of the rest of the assembly. This allowed us to simulate the heat transfer process that results in the simultaneous increase in membrane temperature and heat flux through the ESR. Figure 8 shows the numerical model, and Table 1 lists the layers in the ESR structure with their thermophysical properties.

The temperature of the ESR base and the chamber wall were set at their experimental values of 13 and −195°C, respectively. The initial membrane temperature was set at an arbitrary value of −100°C. The membrane temperature was then changed in a trial and error procedure to match the numerical results to the experimental heat flux values. The best match between the two was achieved at an initial membrane temperature of −20°C, as shown in Fig. 9. A grid-independent solution was obtained with 209,513 nodes. The time steps were nonuniform with a step size of 0.1 s for the first 2 s, which increased in increments to a step size of 1 s for the 8–10 s range.

Uncertainty Analysis

An analysis of the experimental errors was conducted to determine the uncertainty in the emissivity measurements of the ESR. First, the emissivity was calculated assuming the vacuum chamber acts as a blackbody with no radiation reflected back to the test surface. A calculation of emissivity with diffuse radiation was then carried out for a sample set of data using Eq. (2) instead of Eq. (1). In this calculation, the black paint coating the chamber wall was considered to have an emissivity of 0.9, as measured by Sheldahl. With the diffuse radiation model, the emissivity calculated from Eq. (2) differed by less than 0.2% (±0.001) from Eq. (1). This uncertainty is an order of magnitude smaller than the uncertainty due to measurement errors, and so Eq. (1) was used for the remainder of the error analysis.

Another possible error investigated is the effect of radiation from the edges of the structure assembled on the heat flux sensor. This thickness is dominated by the aluminum plate, which has a very low emissivity. Moreover, the area of this region is only 7.2% of the top surface area. Thus, radiation from the edges was considered negligible, and not included in the uncertainty calculation.

The calculation of emissivity in Eq. (1) depends on the measurement of heat flux, surface temperature, and the temperature of the vacuum chamber walls. Therefore, the thermocouple and heat flux sensor calibration errors as well as measurement errors in the data acquisition unit contribute to uncertainty in calculated emissivity. A root-mean-square analysis was used to combine these uncertainties as shown in Eq. (4): Q5

$$\Delta\varepsilon = \sqrt{\left(\frac{\partial\varepsilon}{\partial q''}\Delta q''\right)^2 + \left(\frac{\partial\varepsilon}{\partial T_S}\Delta T_S\right)^2 + \left(\frac{\partial\varepsilon}{\partial T_\infty}\Delta T_\infty\right)^2} \tag{4}$$

The thermocouples used were type K with an uncertainty of ±2.2°C for subzero and ±1.1°C for above-zero temperatures. The heat flux sensors were calibrated by the manufacturer with a calibration accuracy of 3–5%. Because the heat flux sensor measurements also depend on a temperature correction factor, the error in the surface temperature measurement was combined with the heat flux sensor output error (calibration error and data acquisition error) to provide a root-mean-square error for the heat flux. The heat flux error $\Delta q''$ is given in terms of the output error ΔV and the surface temperature error ΔT_S as

$$\Delta q'' = \sqrt{\left(\frac{\partial q''}{\partial V}\Delta V\right)^2 + \left(\frac{\partial q''}{\partial T_S}\Delta T_S\right)^2} \tag{5}$$

Using Eq. (5), the maximum heat flux error was calculated to be ±19 W/m^2 in the steady activated state and ±6.3 W/m^2 in the deactivated state. This corresponds to an emissivity uncertainty of 6.0%, or ±0.043 in the activated state (high effective emissivity) and ±0.015 in the deactivated state (low effective emissivity).

There is also an error due to taking the temperature measurement at the substrate instead of on the emitting surface itself. Although, when measuring the *effective* emissivity of the structure, the exact location of the temperature measurement is not as important as consistency,

Q12

Table 1 ESR layers and properties specified in numerical model

Layer	Layer thickness, m	Thermal conductivity, W/m · K, and/or emissivity	Density, kg/m^3	Specific heat, J/kg · K
Al substrate	4.78×10^{-3}	240	2700	336
Epoxy 1	5×10^{-5}	6.5	1200	1500
Heat flux sensor	2×10^{-4}	0.2	1100	1500
Epoxy 2	5×10^{-5}	6.5	1200	1500
Al baseplate	8.13×10^{-4}	240	2700	336
Al baseplate	2.5×10^{-5}	0.1	500	1200
Membrane	1.5×10^{-5}	$k = 0.2$, $\varepsilon = 0.88$	1100	1500

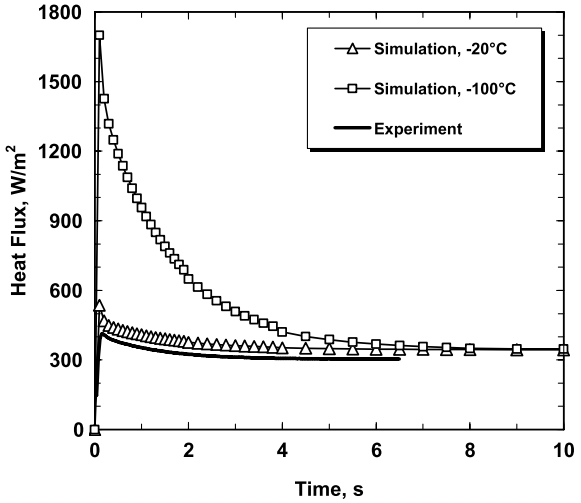

Fig. 9 Comparison of heat flux calculated in ESR transient simulation (with initial membrane temperature of −20 and −100°C) and experimental results.

an additional error can be calculated. The temperature drop from the substrate to the surface can be estimated using simple 1-D conduction. The drop across all layers of the ESR in the activated state is calculated as 1.5°C. This temperature drop contributes an additional biased error (the actual surface temperature is always lower than the substrate temperature while it is emitting heat) of about 1.7%. Adding this temperature drop error to the other measurement errors, the overall root-mean-square error for the emissivity measurements was calculated to be 6.9%.

Conclusions

The HFB emissivity measurement technique was successfully used to study performance of the second-generation ESR device. The transient characteristics of the device were revealed. The fast response time of the measurement technique made possible the study of a delayed release of the ESR membrane at the onset of the deactivation mode. Reversing the applied potential for a short period of time (∼60 s) was found to eliminate the electrostatic memory of the device. A peak in the heat flux during activation was quantified with this technique and compared with a numerical model. This peak is associated with sensible heating of the membrane when it comes into contact with the ESR base surface at the beginning of the activation mode. The second-generation ESR showed a consistent change in emissivity of 0.52 with 280 V applied.

Acknowledgments

The authors acknowledge and appreciate the support provided by the U.S. Air Force SBIR Program Office (under Contracts FA8650-04-M-5020 and FA8650-05-C-5045) and by our technical monitor Ming Chen, U.S. Air Force Research Laboratory, Wright–Patterson Air Force Base. The authors also appreciate William Biter and his coworkers at Sensortex, Inc. for fabricating a series of electrostatic switched radiator devices for this research.

References

[1] Helvajian, H., Janson , S. W., and Robinson, E. Y., "Big Benefits from Tiny Technologies: Micro-Nanotechnology Applications in Future Space Systems," *Critical Reviews of Optical Science and Technology*, Vol. CR66, edited by E. W. Taylor, Society of Photo-Optical Instrumentation Engineers, 1997, pp. 22–23.

[2] Dark, A. G., Osiander, R., Champion, J., Swanson, T., and Douglas, D., "Variable Emissivity Through MEMS Technology," *Proceedings of Space Technology and Applications International Forum (STAIF-2000)*, No. 504, edited by M. El-Genk, AIP Conference Proceedings, American Inst. of Physics, Melville, NY, 2000, pp. 803–808.

[3] Chandrasekhar, P., et al., "Variable Emittance Materials Based on Conducting Polymers for Spacecraft Thermal Control," *Proceedings of the Space Technology and Applications International Forum (STAIF-2003)*, No. 654, edited by M. El-Genk, AIP Conference Proceedings, American Inst. of Physics, Melville, NY, 2003, pp. 157–161.

[4] Kislov, N., Groger, H., and Ponnappan, R., "All-Solid-State Electrochromic Variable Emittance Coatings for Thermal Management in Space," *Proceedings of the Space Technology and Applications International Forum (STAIF-2003)*, No. 654, edited by M. El-Genk, AIP Conference Proceedings, American Inst. of Physics, Melville, NY, 2003, pp. 172–179.

[5] Hale, J. S., and Woollam, J. A., "Prospects for IR Emissivity Control Using Electrochromic Structures," *Thin Solid Films*, Vol. 339, Elsevier, New York, 1999, pp. 174–180.

[6] Osiander, R., et al., "Micromachined Louver Arrays for Spacecraft Thermal Control Radiators," *39th AIAA Aerospace Sciences Meeting & Exhibit*, AIAA Paper 2001-0215, 2001.

[7] Biter, W., Oh, S., and Hess, S., "Electrostatic Switched Radiator for Space Based Thermal Control," *Proceedings of the Space Technology and Applications International Forum (STAIF-2002)*, No. 608, edited by M. El-Genk, AIP Conference Proceedings, American Inst. of Physics, Melville, NY, 2002, pp. 73–80.

[8] Biter, W., Hess, S., and Oh, S., "Electrostatic Appliqué for Spacecraft Temperature Control," *Proceedings of the Space Technology and Applications International Forum (STAIF-2003)*, No. 654, edited by M. El-Genk, AIP Conference Proceedings, American Inst. of Physics, Melville, NY, 2003, pp. 162–171.

[9] Farrar, D., et al., "MEMS Shutters for Thermal Control: Flight Validation and Lessons Learned," *Proceedings of the Space Technology and Applications International Forum (STAIF-2007)*, No. 978, edited by M. El-Genk, AIP Conference Proceedings, American Inst. of Physics, Melville, NY, 2007, pp. 73–80.

[10] Moghaddam, S., Lawler, J., McCaffery, C., and Kim, J., "Heat Flux-Based Emissivity Measurement," *Proceedings of the Space Technology and Applications International Forum (STAIF-2005)*, No. 746, edited by M. El-Genk, AIP Conference Proceedings, American Inst. of Physics, Melville, NY, 2005, pp. 32–37.

[11] Moghaddam, S., Lawler, J., Currano, J., and Kim, J., "Novel Method for Measurement of Total Hemispherical Emissivity," *Journal of Thermophysics and Heat Transfer*, Vol. 21, No. 1, 2007, pp. 128–133. doi:10.2514/1.26181

[12] Biter, W., and Oh, S., "Performance Results of the ESR from the Space Technology 5 Satellites," *Proceedings of the Space Technology and Applications International Forum (STAIF-2007)*, No. 880, edited by M. El-Genk, AIP Conference Proceedings, American Inst. of Physics, Melville, NY, 2007, pp. 59–65.

[13] Lasance, C. J. M., "Thermal Conductivity of Air at Reduced Pressures and Length Scales," *Electronics Cooling Online* [online periodical], Nov. 2002, http://electronics-cooling.com/articles/2002/2002_november_techdata.php [cited 24 Aug. 2007].

[14] Scott, R. B., *Cryogenic Engineering*, edited by D. Van Norstrand, Princeton, NJ, 1959, pp. 144–146.

[15] Brewster, M. Q., *Thermal Radiative Transfer and Properties*, Wiley, New York, 1992, p. 89.

Queries

IMPORTANT: PLEASE READ CAREFULLY.

When production of AIAA journal papers begins, the official approved PDF is considered the authoritative manuscript. Authors are asked to submit source files that match the PDF exactly, to ensure that the final published article is the version that was reviewed and accepted by the associate editor. Once a paper has been accepted, any substantial corrections or changes must be approved by the associate editor before they can be incorporated.

If you and the EIC settled on some final changes to your manuscript after it was accepted, it is possible that your page proofs do not reflect these final changes. If that is the case, please submit these changes as itemized corrections to the proofs.

If final changes were made to the figures, please check the figures appearing in the proofs carefully. While it is usual procedure to use the figures that exist in the source file, if discrepancies are found between figures (manuscript source file vs the approved PDF), the figures from the PDF are inserted in the page proofs, again deferring to the PDF as the authoritative manuscript. If you find that agreed-upon final changes to your figures are not appearing in your page proofs, please let us know immediately.

Q1. Please check the copyright statement in the first page footnote to ensure accuracy. Please include any AIAA membership to be included in the authors' footnotes.
Q2. Acronyms must be defined the first time they are used. We have defined MEMS as microelectromechanical sensor. Is this correct?
Q3. Fractions in the denominator have been expanded, per AIAA style. Please check to ensure the meaning of the equation has not been changed.
Q4. Please supply a definition for PID.
Q5. Equations (6,7) in the manuscript were changed to Eqs. (4,5) so that equations appear in numerical order.
Q6. Please supply a definition for SBIR.
Q7. Please provide a location for the publisher in [1].
Q8. In the reference list, "et al." is not used, per AIAA style. Please list all authors for [3, 6, 9].
Q9. Please provide the publisher for [14].
Q10. AIAA style indicates that figure captions should be 12 words or less. Please consider shortening the captions of Figs. 4, 5, 9, by moving information to the text where the figure is cited, or by removing duplicated information.
Q11. Please supply a definition for VDC in Fig. 6.
Q12. It was necessary to retype the information in Table 1. Please check carefully for errors.